Untargeted and targeted metabolomics profiling reveals the underlying pathogenesis and abnormal arachidonic acid metabolism in laying hens with fatty liver hemorrhagic syndrome

Jiacheng Meng,[*,1] Ning Ma,[*,†,1] Hailong Liu,[‡] Jing Liu,[*] Juxiang Liu,[*] Jianping Wang,[*] Xin He,[*] and Xinghua Zhao[*,2]

[*]*College of Veterinary Medicine, Hebei Agricultural University, Baoding 071001, Hebei, China;* [†]*Hebei Veterinary Biotechnology Innovation Center, Baoding 071001, Hebei, China; and* [‡]*Hainan Academy of Agricultural Sciences, Haikou 571100, Hainan, China*

ABSTRACT As a metabolic disease, fatty liver hemorrhagic syndrome (**FLHS**) has become the major factor responsible for the noninfectious cause of mortality in laying hens, which lead to huge economic losses to poultry industry. However, the pathogenesis of FLHS remains unclear. The aim of present study was to identify novel liver metabolites associated with FLHS. Twenty healthy Chinese commercial Jing Fen laying hens aged 90 d were used in present study. After acclimatization for 2 wk, the hens were divided into 2 treatments (n = 10): control group (normal diet) and FLHS group (high-energy low-protein diet). The experiment lasted for 48 d, and the laying hens were killed for blood and liver sampling at the end of the experiment. Blood biochemical indicators and liver pathological changes were examined. Meanwhile, the changes in liver metabolic profile were investigated with the application of metabolomics approach. Significant increased levels of alanine aminotransferase, aspartate aminotransferase, low density lipoprotein, total cholesterol and triglycerides, decreased high density lipoprotein ($P < 0.01$), and hepatic steatosis were observed in hens of FLHS group, which suggested FLHS was successfully established in this study. Distinct changes in metabolite patterns in liver between control and FLHS group were observed by partial least-squares discriminant analysis. In total, 42 liver metabolites including tyrosine, glutathione, carnitine, linoleic acid, uric acid, arachidonic acid (**ARA**), lactate and lysophosphatidylcholine (14: 0) were identified and considered to be related with pathogenesis of FLHS. Pathway analysis revealed that these metabolites were mainly involved in amino acid metabolism, fatty acid metabolism, ARA metabolism, glucose metabolism and glycerophospholipid metabolism. Furthermore, targeted metabolomics found that ARA metabolites such as prostaglandins and hydroxyeicosatetraenoic acids were significantly increased in FLHS group ($P < 0.05$). In conclusion, our data showed that liver metabolites and ARA metabolism were linked to the pathophysiology of FLHS, which provided a basis for understanding the pathogenesis of FLHS in laying hens.

Key words: fatty liver hemorrhagic syndrome, arachidonic acid, metabolomic, liver, mass spectrometry

2021 Poultry Science 100:101320
https://doi.org/10.1016/j.psj.2021.101320

INTRODUCTION

As a metabolic disease, fatty liver hemorrhagic syndrome (**FLHS**) is caused by many factors such as diet ratio, hormones, genetics and environment (Trott et al., 2014). Characterized by the accumulation of lipid and fat, FLHS frequently occurs in caged high-production and overconditioned laying hens. It has been reported that FLHS is the major factor responsible for the noninfectious cause of mortality in laying hens (Shini et al., 2019). Moreover, FLHS can cause sudden death and sharp drop in egg production rate, which result in serious economic losses to laying hens industry (Lee et al., 2010). As a metabolic disease, FLHS has a great similarity to nonalcoholic fatty liver disease (**NAFLD**) in human beings (Hamid et al., 2019). The common pathologic features of FLHS and NAFLD are excess hepatic lipid deposition. Previous studies have provided that pathogenic causes such as inflammation, lipid disorder, oxidative stress, autophagy, and gut microbiota are related to FLHS (Gao et al., 2019; Xing et al., 2020).

Received April 27, 2021.
Accepted June 4, 2021.

[1]These authors contributed equally to this study.

[2]Corresponding author: xianzhaoxinghua@163.com

However, the exact pathogenesis underlying FLHS have not been fully elucidated. It has been found that the changes of metabolites can provide new evidence to illustrate the disease pathogenesis.

As the final downstream products of gene transcription, metabolites play a key role in disease, and can directly reflect the actual functional endpoints of biological events. By measuring the changes of metabolites, metabolomics offers fresh insights into the disease pathogenesis (Johnson et al., 2016). With the application of gas chromatography-mass spectrometry based metabolomics, the researchers found that some liver metabolites participated in FLHS (Zhuang et al., 2019), and serum metabolites could be used in the clinical diagnosis of FLHS (Guo et al., 2021). Due to the high resolution, powerful separation and excellent sensitivity, ultraperformance liquid chromatography-quadrupole time-of-flight mass spectrometry (**UPLC-QTOF/MS**) has been proved to be an indispensable technique for metabonomic analysis. However, to our knowledge, there was no report related to metabolomic study performed by UPLC-QTOF/MS in FLHS. Therefore, UPLC-QTOF/MS based metabolomics analysis might be attractive for metabolites investigation, which can provide a new insight into the pathogenesis of FLHS. From the perspective of metabolism, identification of the key metabolites and the analysis of their related pathway can contribute to understanding the possible pathogenesis of FLHS.

As an omega-6 polyunsaturated essential fatty acid, arachidonic acid (**ARA**) is a critical metabolite in liver and plays essential roles in many pathological and physiological processes (Tallima and El, 2018). ARA is synthesized from linoleic acid and studded in biological cell membrane, so the concentration of free ARA in cells is very low. Activated phospholipase A2 can cleave ARA from the cell membrane, and then the free ARA will be metabolized by cyclooxygenase, lipoxygenase, and cytochrome P450 enzymes (Liu et al., 2019). It is well known that the major action of the metabolites derived from ARA is to promote the acute inflammation through the production of proinflammatory mediators such as prostaglandins and leukotrienes. Therefore, ARA is a precursor to proinflammatory mediators and makes a significant contribution to inflammation. Severe hepatic and systemic inflammation have been observed in laying hens with FLHS (Shini et al., 2020). It is speculated that ARA metabolism participates the pathogenesis of FLHS through the regulation of inflammation. Additionally, recent studies have indicated that a variety of biologically active metabolites produced by ARA also have a close relationship with oxidative stress, lipid metabolism, and immune function (Hadley et al., 2016; Sonnweber et al., 2018). It has been demonstrated that ARA metabolism plays an important role in the occurring and development of NAFLD (Arendt et al., 2015; Sztolsztener et al., 2020). For the similar pathogenesis of NAFLD and FLHS, it is interesting to explore the relationship of ARA metabolism and FLHS. However, it is unknown whether ARA metabolites are changed in liver from laying hens with FLHS.

The objective of present study was to identify novel liver metabolites associated with FLHS in laying hens. Through the application of untargeted and target UPLC-QTOF/MS based metabolomics, the specific metabolites and related pathways were identified. Meanwhile, the disturbance of ARA metabolism was observed in FLHS. These findings might help to facilitate a better understanding of FLHS and gain new insights into the pathogenesis of FLHS.

MATERIALS AND METHODS

Animals and Treatments

Twenty healthy Chinese commercial Jing Fen laying hens aged 90 d were purchased from the local hen farm. The hens were raised for 2 wk for acclimatization, and then equally divided into 2 groups: the control group and the FLHS group (n = 10). The hens in FLHS group were induced by the high-energy low-protein diet as described in the previous studies (Gao et al., 2019; Zhuang et al., 2019). The detailed composition of the diets for the hens was shown in Supplementary Table 1. The experiment was lasted for 48 d. All the experimental protocols were approved by Institutional Animal Care and Use Committee of Hebei Agricultural University and carried out in accordance with the Guidelines of the Care and Use of Laboratory Animals of China.

Sample Collection

At the end of the experiment, all the hens were fasted for 12 h before weighing and blood sampling. Blood samples were collected from the brachial vein into vacuum tubes to obtain serum (4000 × *g*, 4°C for 10 min), and then be stored at -20°C for lipid analysis. The hens were anesthetized and sacrificed after blood collection. The liver was carefully removed and weighted. A portion of liver tissue was fixed in 4% formalin for observations of pathological changes, and the remaining liver tissue was snap-frozen in liquid nitrogen and then stored at −80°C for metabolomics analysis.

Blood Lipids and Pathological Examination

The levels of alanine aminotransferase (**ALT**), aspartate aminotransferase (**AST**), high density lipoprotein (**HDL**), low density lipoprotein (**LDL**), triglycerides (**TG**), and total cholesterol (**TCH**) in serum were determined by assay kits (Shanghai Jiang Lai bio-technology Co., Ltd., Shanghai, China). Under the standard protocol, tissues of liver were formalin-fixed and paraffin embedded, sectioned, and stained with hematoxylin and eosin (**HE**). Meanwhile, routine oil red O method was used to investigate the lipid droplet accumulation in liver. Stained sections by HE and oil red O were examined using CX31 biological microscope (Olympus Corporation, Tokyo, Japan).

Liver Metabolite Extraction

Liver samples were thawed at room temperature prior to analysis. Liver tissue of 80 mg was precisely weighted, and then 1 mL of cold methanol/acetonitrile/H_2O (2:2:1, v/v/v) was added. The mixture was adequately vortexed and homogenized for 1 min. Then, the homogenate was sonicated at low temperature (30 min/once, twice) to extract the compounds from liver. Next, the samples were incubated for 1 h at -20°C to precipitate the protein, and be centrifuged at 14,000 *g* for 20 min at 4°C. The supernatant was collected and dried. Lyophilized powder samples were redissolved in 100 μL acetonitrile/water (1:1, v/v) solvent for metabolomic analysis. Quality control (**QC**) samples pooled from all liver tissue samples were prepared and analyzed with the same procedure.

Untargeted Metabolomics Data Acquisition and Processing

The liver sample was analyzed on a quadrupole time-of-flight mass spectrometry (Agilent Q-TOF 6550) coupled with Agilent 1290 high-performance liquid chromatograph system (Agilent Technologies Inc., Palo Alto, CA). Chromatographic separation of liver tissue was performed on a ACQUIY UPLC BEH column (2.1 × 100 mm, 1.7 μm, Waters Corporation, Milford, MA). The column was maintained at 25°C and eluted at a flowing rate of 0.3 mL/min. The mobile phase was consisted of A (25 mM ammonium acetate and 25 mM ammonium hydroxide in water) and B (acetonitrile) with the gradient: 0−0.5 min, 95% B; 0.5−7 min, 95−65% B; 7−8 min, 65−40% B; 8−9 min, 40% B; 9−9.1 min, 40−95% B, 9.1−12 min, 95% B. Mass spectrometry (**MS**) data was acquired through Agilent Q-TOF 6550 with a dual electrospray ionization (**ESI**) source operating in positive (ESI+) and negative ion (ESI-) modes. The main operation parameters of the mass spectrometer were set as follows: gas temperature, 250°C; drying gas, 16 L/min; nebulizer, 20 psig; sheath gas temperature, 400°C; sheath gas flow: 12 L/min, Vcap voltage, 3000 V; nozzle voltage, 0 V; fragment voltage, 175 V; mass range, 50−1200; acquisition rate, 4 Hz; cycle time, 250 ms.

Metabolite Identification and Pathway Analysis

Structure identification of metabolites was performed by comparing of accuracy m/z value (<25 ppm) and MS/MS spectra with an in-house database established by available authentic standards. Metabonomic pathway analysis was performed by MetaboAnalyst 5.0 (https://www.metaboanalyst.ca/MetaboAnalyst/), the impact-value calculated from the pathway analysis was set to 0.10, and the metabolic pathways with impact-value above 0.10 were selected out. In addition, affected biochemical reactions were identified by KEGG database (http://www.kegg.jp/) for further biochemical interpretation.

ARA Targeted Metabolomics Analysis

In order to determine the changes of ARA metabolites in the layers from control and FLHS groups, the quantitative analysis of ARA metabolites in liver was performed by targeted metabolomics. Quantitative analysis of ARA metabolites including prostaglandin (**PG**) F2α (**PGF2α**), PGE2, PGD2, 8-isoprostaglandin F2α (**8-iso-PGF2α**), thromboxane B2 (**TXB2**), docosahexaenoic acid (**DHA**), 15(S)-hydroxyeicosatetraenoic acid (**15S-HETE**), 12S-HETE, 13(S)-hydroxyoctadecadienoic acid (**13S-HODE**), and 9S-HODE was performed in present study. A Waters I-class liquid chromatography system (Waters Corporation, Milford, USA) coupled with QTRAP 5500 (AB SCIEX, Boston, MA) mass spectrometer was used in the ARA targeted metabolomics. The mass spectrometer was operated in the negative ionization mode with multiple reaction monitoring (**MRM**) method. A 4 μL aliquot of each sample was injected for analysis. The chromatographic separation of ARA metabolites was performed using a RP18 column (2.1 × 50 mm, 1.7 μm, Waters ACQUITY BEH Sheid, Milford, MA). The column was maintained at 45°C and eluted at a flowing rate of 0.4 mL/min. The mobile phase consisted of phase A (0.1% formic acid in water) and phase B (0.1% formic acid in acetonitrile) with following method: 0−1 min, 30% B; 1−7 min, 30−80% B; 7−9 min, 80−90% B; 9−11 min, 90% B. The conditions of mass spectrometer were set as follows: source temperature 450°C, ion source gas 1: 55, ion source gas 2: 60, curtain gas: 30, ion sapary voltage floating: -4500 V. Response curve, retention time and MRM transition of each ARA metabolite were provided in Supplementary Table 2.

Statistical Analysis

For untargeted metabolomics data analysis, the raw MS data were converted to mzXML files using ProteoWizard. The XCMS program was used for nonlinear alignment, automatic integration and extraction of the peak intensities. After normalized to total peak intensity, the data were processed by SIMCA-P (Umetrics AB, Umea, Sweden). For multivariate data analysis, Pareto-scaled principal component analysis (**PCA**) and partial least-squares discriminant analysis (**PLS-DA**) were performed. Capability of PCA and PLS-DA models were described by cumulative R^2 and Q^2. In order to avoid overfitting, the permutation test (200 times) of PLS-DA models were performed. Potential metabolites were identified according to the variable importance in the projection (**VIP**) value obtained from PLS-DA model and the *P*-value from Student's t-test. Metabolite with VIP > 1 and $P < 0.05$ was considered as statistically significant.

Table 1. Liver index and blood lipid results of layers in control and FLHS groups.

Variables	Control	FLHS
Liver index, %	1.96 ± 0.31	2.43 ± 0.28**
TCH, mmol/L	33.6 ± 3.86	59.8 ± 6.05**
TG, mmol/L	2.35 ± 0.49	5.02 ± 0.55**
HDL, μmol/L	1209.7 ± 192.47	741.62 ± 67.77**
LDL, mmol/L	5.76 ± 0.51	8.89 ± 0.88**
ALT, mmol/L	83.32 ± 27.8	246.65 ± 18.81**
AST, mmol/L	251.93 ± 31.9	542.7 ± 36.2**

Abbreviations: ALT, alanine transaminase; AST, aspartate aminotransferase; HDL, high-density lipoprotein; LDL, low-density lipoprotein; Liver index (%), liver weight/body weight × 100%; TCH, total cholesterol; TG, triglyceride.
** $P < 0.01$, compared with the control group.

The results of blood biochemical indicators were expressed as mean ± SD. Statistical comparisons between control group and FLHS group was analyzed by Student's t test of SPSS 16.0 (SPSS Inc., Chicago, IL). P-values below 5% were considered significant.

RESULTS

Blood Lipid Analysis

Table 1 shows the results of liver index and blood lipids. Liver index of the layers in FLHS group significantly increased than that in the control group ($P < 0.01$). Compared with the control layer, the concentrations of TG, TCH, and LDL in plasma were significantly increased, while HDL was decreased in the layers with FLHS ($P < 0.01$). Furthermore, plasma ALT and AST levels in the layers from FLHS group were significantly higher than those in the control ($P < 0.01$).

Hepatic Histopathology

Histological examinations of the hepatic tissue of the layers in control and FLHS groups are shown in Figure 1. Hepatic tissues were stained with HE (Figure 1, A and B) and oil red O (Figure 1, C and D). Clear and normal liver cell architecture was observed in healthy layers from the control group. However, steatosis and necrosis were found in the FLHS group. Severe fatty degeneration and lipid droplet accumulation in liver cells were observed in layers from FLHS group.

Liver Untargeted Metabolomics Profile of FLHS

In present study, pooled QC samples were used during the sample analysis to validate the system performance. PCA in ESI positive mode and negative mode were performed on all samples in the study (Supplementary Figure 1). There QC samples were tightly clustered in the PCA score plots in both modes, which demonstrated the metabolomic method was robust with good repeatability and stability. Liver samples of the layers in the

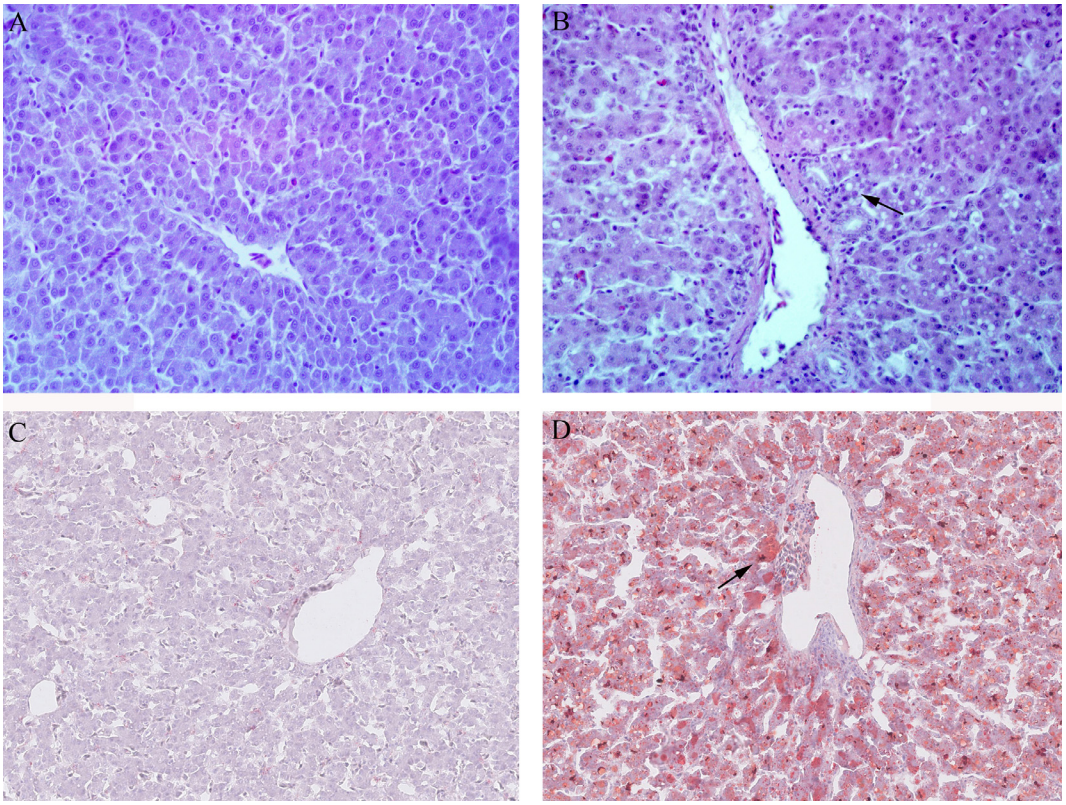

Figure 1. Histological changes in liver sections stained with HE and oil red O of the layers in control and FLHS groups (200 × magnification). Liver tissue from control (A) and FLHS group (B) by HE staining; Liver tissue from control (C) and FLHS group (D) by oil red staining. Fatty degeneration and fat droplet (arrow-labeled) were found in the liver cells in FLHS group. Abbreviation: FLHS, fatty liver hemorrhagic syndrome; HE, hematoxylin and eosin.

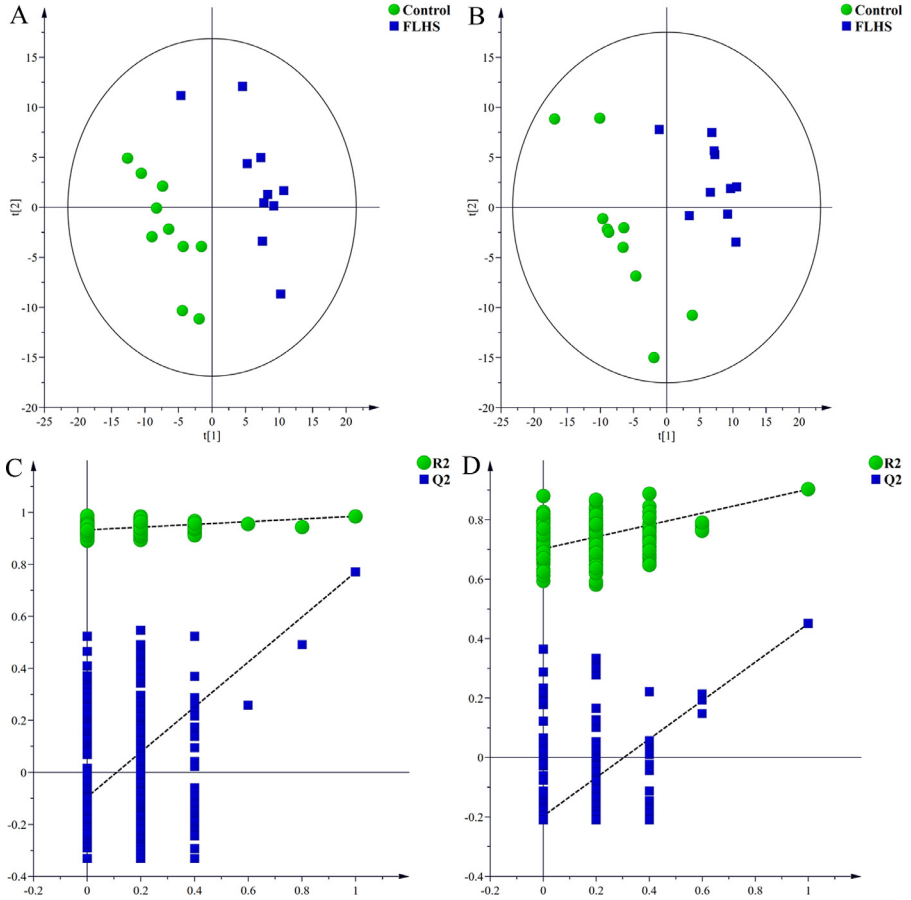

Figure 2. PLS-DA score plots and permutation test derived from the liver tissue of layers in control and FLHS groups. (A and B) PLS-DA score plots between control and FLHS groups in positive and negative modes, respectively. (C and D) Plot of the permutation test of PLS-DA modes in positive and negative modes, respectively. Abbreviations: FLHS, fatty liver hemorrhagic syndrome; PLS-DA, partial least-squares discriminant analysis.

FLHS group showed a tendency to be away from those in the control group in the PCA score plots (Supplementary Figure 1), which revealed the disorders of live metabolic profile in the layers with FLHS.

Next, PLS-DA was conducted to identify the potential metabolites that were different between the control and FLHS groups. Clear separate clustering patterns between control group and FLHS group were found by PLS-DA score plots in ESI+ (R^2X = 0.382, R^2Y = 0.985, Q^2 = 0.771) and ESI- (R^2X = 0.372, R^2Y = 0.957, Q^2 = 0.444) (Figure 2 A and B). In PLS-DA score plots, FLHS group showed a trend to be away from the control group, indicating the distinguishable changes in the liver from FLHS group at the metabolite level. Two hundred random permutation tests were applied to guard against PLS-DA model overfitting. Results of the permutation test showed that the intercepts of R^2 = 0.929 and Q^2 = -0.143 for positive model (Figure 2C) and R^2 = 0.860 and Q^2 = -0.232 for negative model (Figure 2D), which indicated that the PLS-DA models were robust without overfitting.

Based on the *P*-value (<0.05) from Student's *t* test and VIP-value (> 1) from PLS-DA models, 42 liver metabolites were selected and identified (Table 2), among which 24 metabolites were significantly increased and 18 metabolites were reduced in FLHS group in comparison with the control group. Among these metabolites, the levels of cytidine, isomaltose, lysophosphatidylcholine (**LysoPC**) (14:0), 1-palmitoylglycerol, LysoPC (16:0), glutathione, linoleoyl ethanolamide, maltose, myo-Inositol, hypoxanthine, inosine, lysophosphatidylethanolamine (**LysoPE**) (16:0), linolenic acid, linoleic acid, myristic acid, lactose, ascorbic acid, maltotriose, lactate, O-phosphoethanolamine, sucrose, glutaric acid, pyruvaldehyde, and allose were increased in the FLHS group, and the levels of tyrosine, 1-methylhistamine, uracil, glutathione disulfide, stearoylcarnitine, betaine aldehyde, cytosine, carnitine, 5-hydroxyindoleacetate, 7-methylxanthine, kynurenine, MHPG-sulfate, uric acid, arachidonic acid, p-Cresol, gamma-glutamylglutamic acid, dihydrothymine, and allantoin were reduced. According to the relative abundance of the liver metabolites, hierarchical clustering analysis was performed to generate a heatmap to show a global view of the metabolites (Figure 3A). The horizontal axis of heatmap showed that the metabolites with similar abundance pattern were clustered together, and the vertical axis of the heatmap showed the liver samples were mainly gathered in 2 clusters.

Summary of the results of metabolic pathway analysis is provided in Supplementary Table 3. The disturbed pathways in response to FLHS were shown in

Table 2. Identification results of different metabolites in liver between control and FLHS groups.

NO.	Metabolite	Adduct	m/z	RT(s)	VIP	FC	*P*-value
1	Tyrosine	$(M+H)^+$	182.0783	251.83	1.84	0.37	0.0002
2	1-Methylhistamine	$(M+H)^+$	126.1021	113.53	2.21	0.45	0.0006
3	Uracil	$(M+H)^+$	113.0343	174.55	1.71	0.62	0.0017
4	Oxidized glutathione	$(M+H)^+$	613.1573	490.07	4.59	0.63	0.0094
5	Stearoylcarnitine	$(M-H+2Na)^+$	472.3387	166.18	1.53	0.48	0.0108
6	Cytidine	$(M+H)^+$	244.0928	236.12	3.73	1.82	0.0128
7	Betaine aldehyde	$(M+H)^+$	102.0922	299.14	11.02	0.51	0.0165
8	Isomaltose	$(M+NH_4)^+$	360.1478	385.51	2.39	4.36	0.0234
9	LysoPC (14:0)	$(M+H)^+$	468.3053	196.18	1.09	1.67	0.0239
10	1-Palmitoylglycerol	$(M+H-H_2O)^+$	313.2718	197.80	1.33	2.15	0.0253
11	Cytosine	$(M+H)^+$	112.0504	170.94	1.85	0.61	0.0280
12	LysoPC (16:0)	$(M+H)^+$	496.3390	192.12	17.36	1.52	0.0286
13	Glutathione	$(M+H)^+$	308.0895	426.11	1.97	1.61	0.0321
14	Linoleoyl ethanolamide	$(M+H)^+$	324.2884	36.20	2.06	1.50	0.0355
15	Carnitine	$(M+H)^+$	162.1122	375.10	5.31	0.59	0.0357
16	Maltose	$(M+H-H_2O)^+$	325.1116	447.07	2.22	6.50	0.0363
17	Myo-inositol	$(M-H)^-$	179.0557	359.90	1.07	2.60	0.0007
18	Hypoxanthine	$(M-H)^-$	135.0320	163.09	14.35	2.85	0.0023
19	Inosine	$(M-H)^-$	267.0727	214.15	2.33	2.51	0.0024
20	5-Hydroxyindoleacetate	$(M-H)^-$	190.0504	257.31	1.98	0.28	0.0029
21	LysoPE (16:0)	$(M-H)^-$	452.2764	198.02	5.90	2.48	0.0070
22	7-Methylxanthine	$(M+CH_3COO)^-$	225.0626	442.02	1.50	0.51	0.0084
23	Kynurenine	$(M-H)^-$	207.0767	257.01	1.29	0.27	0.0085
24	MHPG-sulfate	$(M-H)^-$	263.0219	41.28	2.10	0.56	0.0089
25	Linolenic acid	$(M-H)^-$	277.2166	41.57	9.61	2.20	0.0110
26	Linoleic acid	$(M-H)^-$	279.2331	41.08	43.07	1.65	0.0138
27	Uric acid	$(M-H)^-$	167.0215	325.13	4.13	0.58	0.0171
28	Arachidonic acid	$(M-H)^-$	303.2327	38.64	20.27	0.68	0.0180
29	Myristic acid	$(M-H)^-$	227.2011	43.81	6.07	1.71	0.0188
30	Lactose	$(M-H)^-$	341.1075	385.97	2.20	4.39	0.0196
31	Ascorbic acid	$(M+Na-2H)^-$	197.0066	124.01	1.12	1.96	0.0216
32	Maltotriose	$(M+CH_3COO)^-$	563.1811	445.62	1.17	5.84	0.0226
33	Lactate	$(M-H)^-$	89.0242	253.76	2.10	1.82	0.0240
34	p-Cresol	$(M-H)^-$	107.0499	45.53	1.00	0.31	0.0250
35	O-Phosphoethanolamine	$(M-H)^-$	140.0116	465.68	2.09	6.88	0.0273
36	Sucrose	$(M-H)^-$	341.1077	448.11	2.07	4.43	0.0276
37	Glutaric acid	$(M-H)^-$	131.0345	297.89	1.06	1.53	0.0346
38	Gamma-Glutamylglutamic acid	$(M-H)^-$	275.0888	454.23	1.78	0.74	0.0405
39	Dihydrothymine	$(M+K-2H)^-$	165.0053	282.72	1.96	0.57	0.0420
40	Allantoin	$(M-H_2O-H)^-$	139.0258	297.51	1.76	0.64	0.0457
41	Pyruvaldehyde	$(2M-H)^-$	143.0345	297.61	1.51	1.49	0.0471
42	Allose	$(M-H)^-$	179.0555	257.51	1.94	2.28	0.0487

Abbreviations: FC, fold change, FLHS group vs. control group; FLHS, fatty liver hemorrhagic syndrome; LysoPC, Lysophosphatidylcholine; MHPG-sulfate, 3-methoxy-4-hydroxyphenylglycol sulfate; RT, retention time; VIP, variable importance in the projection.

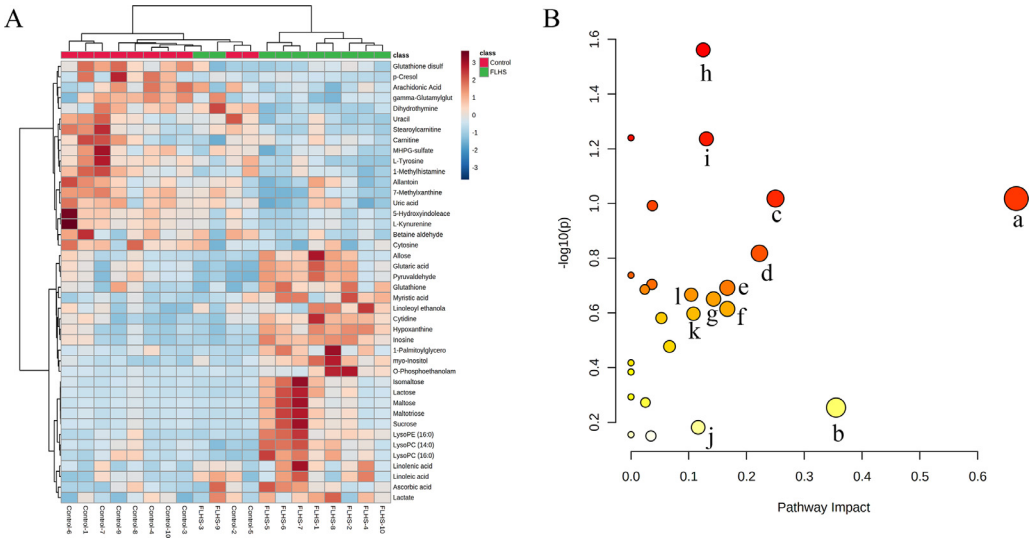

Figure 3. Heatmap and pathway analysis of identified liver metabolites related to FLHS. (A) Heatmap of the 42 different liver metabolites in control and FLHS groups. Red color indicates the metabolites with high relative abundance, and the blue color indicates low relative abundance. (B) Disturbed pathways in response to FLHS. Pathways with the impact value >1 were labeled: a, linoleic acid metabolism; b, arachidonic acid metabolism; c, phenylalanine, tyrosine and tryptophan biosynthesis; d, glutathione metabolism; e, ubiquinone and other terpenoid-quinone biosynthesis; f, caffeine metabolism; j, ascorbate and aldarate metabolism; h, starch and sucrose metabolism; i, galactose metabolism; j, tyrosine metabolism; k, tryptophan metabolism; l, glycerophospholipid metabolism. Abbreviation: FLHS, fatty liver hemorrhagic syndrome.

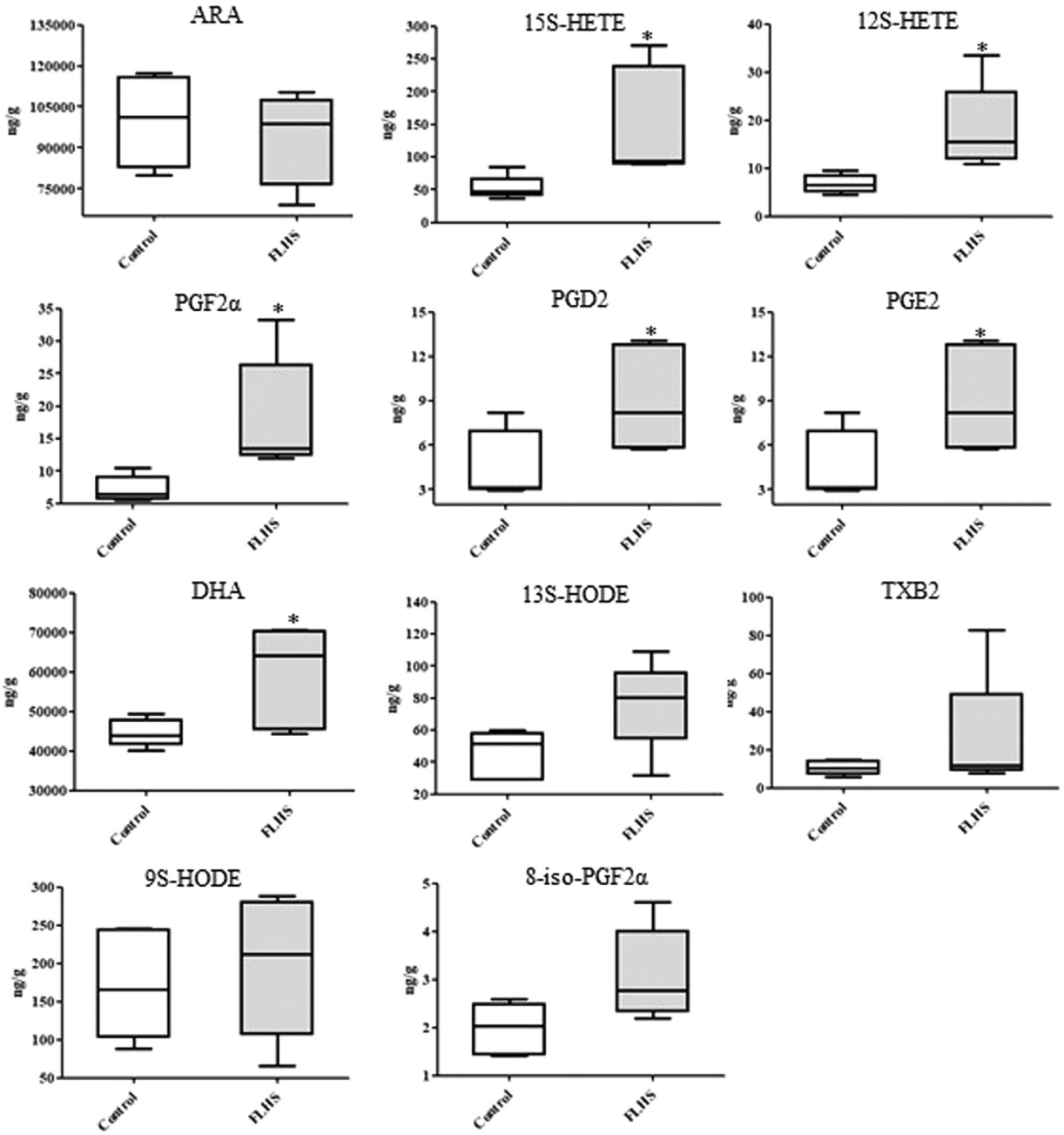

Figure 4. Concentrations of liver metabolites involved in ARA metabolism by targeted analysis. Abbreviations: ARA, arachidonic acid; 15S-HETE, 15(S)-hydroxyeicosatetraenoic acid; 12S-HETE, 12(S)-hydroxyeicosatetraenoic acid; PGF2α, prostaglandin F2α; PGD2, prostaglandin D2; PGE2, prostaglandin E2; DHA, docosahexaenoic acid; 13S-HODE, 13(S)-hydroxyoctadecadienoic acid; TXB2, thromboxane B2; 9S-HODE, 9(S)-hydroxyoctadecadienoic acid; 8-iso-PGF2α, 8-isoprostaglandin F2α. * $P < 0.05$, compared with the control group.

Figure 3B, which indicated that the metabolic pathways such as glycerophospholipid metabolism, tryptophan metabolism, ARA metabolism, tyrosine metabolism, galactose metabolism, starch and sucrose metabolism, biosynthesis of unsaturated fatty acids, phenylalanine, tyrosine and tryptophan biosynthesis, linoleic acid metabolism, pyruvate metabolism and glutathione metabolism were responsible for FLHS. Interestingly, the pathway impact-value of ARA metabolism was 0.336, which might play an important role in FLHS. Therefore, we further investigated the changes of ARA metabolites in the liver of layers with FLHS.

ARA Targeted Metabolomic Study

Results of quantitative analysis of ARA metabolites are shown in Figure 4. In FLHS group, the mean level of ARA was lower than that in the control, but the difference was not statistically significant in the experiment ($P > 0.05$). When compared with the control group, it was found that the levels of 15S-HETE, 12S-HETE, PGF2α, PGD2, PGE2 and DHA were markedly increased in FLHS group ($P < 0.05$), and the mean levels of 13S-HODE, TXB2, 9S-HODE, and 8-iso-PGF2α in FLHS group were also higher (Figure 4), but not reaching statistical significance.

DISCUSSION

Disorders of lipid metabolism are a key risk factor for FLHS. Increased TCH, TG, LDL, ALT and AST and decreased HDL were found in present study, which indicated that the blood lipid profile in FLHS group was significantly changed by high-energy low-protein diet. In blood stream, LDL is responsible for cholesterol transportation, and HDL is the mediator for the excretion of cholesterol from the body (Xu et al., 2013). When the liver cells damaged, the important transaminases such as AST and ALT are released into the blood by liver. Gao et al. found that the plasma levels of TG, TCH, LDL, AST, and ALT were significantly increased in the laying hens with FLHS than those in the control group, and HDL was extremely decreased (Gao et al., 2019). In addition, pathological injuries such as steatosis, necrosis and lipid droplet accumulation were observed in liver from FLHS group through HE and oil red O staining. Fatty degeneration is typical pathological characteristic of liver in layers with FLHS. Pathological observation and blood lipid results in FLHS group in this study were agreed with each other, indicating the FLHS model induced by high-energy low-protein diet was established successfully in this study.

With the application of FLHS model, untargeted UPLC-QTOF/MS metabolomics study of liver was performed to investigate the pathological mechanism of FLHS. The results found that the metabolic profile of liver in the FLHS group deviated from the control, which suggested the significant changes of liver metabolites in the layers with FLHS. Especially 42 biomarkers such as lactose, carnitine, tyrosine, LysoPC (14:0), linoleic acid, glutathione, and ARA associated with FLHS were identified. Pathway analysis showed that these metabolites were mainly involved in glucose metabolism, fatty acid metabolism, amino acid metabolism, glycerophospholipid metabolism, glutathione metabolism, and ARA metabolism. Changes of these liver metabolites and the altered metabolic pathways may provide new evidence to understand the pathogenesis of FLHS.

Disorder of glucose metabolism is a contributor to the pathogenesis of NAFLD. In this study, levels of maltose, lactose and sucrose were increased in the FLHS group. Glucose metabolism was found to be up-regulated in the liver of mice or human with NAFLD (Saely et al., 2017; Lu et al., 2020). Moreover, fasting glucose concentrations were also significantly elevated in the layers fed with high-energy low-protein diet (Zhuang et al., 2019). Long time consumption of high-energy low-protein diet leads to the increase of carbohydrate, and the redundant carbohydrate can be converted to glycogen, which might be the reasons for the increased maltose, lactose and sucrose in the liver. In present study, lactate and pyruvaldehyde involved in pyruvate metabolism were increased in liver in the FLHS group. Lactate was proved to be increased and accumulated with the severity of liver disease such as NAFLD and nonalcoholic steatohepatitis (Jeppesen et al., 2013; Ha et al., 2016). As a cytotoxic and mutagenic product, pyruvaldeheye is derived from increased glycolysis. Damaging roles of lactate and pyruvaldeheye in the liver have been described that they can trigger zinflammation, oxidative stress, mitochondrial impairment and cell death (de Bari et al., 2019; Wang et al., 2021). Therefore, increased lactate and pyruvaldeheye could aggravate the liver damage in the layers, which might facilitate the development of FLHS.

Carnitine and stearoylcarnitine were reduced in the liver in the layers with FLHS in present study. As an essential factor in fatty acid metabolism, carnitine plays key roles in the transportation of fatty acid into mitochondria for oxidation. Under the conditions of fatty liver disease, fatty acid oxidation was promoted to provide energy, which was accompanied with consume of carnitine (Liu et al., 2014). Reduced carnitine and stearoylcarnitine might suggest that fatty acid oxidation was promoted in the liver in the progression of FLHS. In present study, increased levels of linolenic acid and linoleic acid were also found in the FLHS group. Linolenic acid and linoleic acid are essential fatty acids. Wang et al. reported that linoleic acid supplementation could reduce lipid accumulation in the liver and egg in laying hens through regulation the expression of hepatic low-density lipoprotein receptor and 3-hydroxy-3-methylglutaryl coenzyme A reductase (Wang et al., 2019). Meanwhile, biosynthesis of unsaturated fatty acids was reported to be up-regulated in the liver of the rats with hepatic steatosis induced by ethanol (Guo et al., 2017). Therefore, increased linolenic acid and linoleic acid might suggest that the biosynthesis of unsaturated fatty acids was positively related to FLHS in the layers.

Amino acid metabolism is closely associated with hepatic lipidosis. In this study, tyrosine was reduced in the liver tissue suggesting the disorder of amino acid metabolism in FLHS layers. In turkey or mice with fatty liver disease, tyrosine concentration was increased in blood and decreased in the liver, respectively (Middendorf et al., 2019; Liu et al., 2021). The lack of protein in the high-energy low-protein diet might be the main reason for the reduced tyrosine. LysoPC, the oxidation product of low-density lipoprotein, can induce inflammation, autoimmune response and oxidative stress in various diseases including cancer, atherosclerosis, hyperlipidemia and nonalcoholic steatohepatitis (Hsu et al., 2011; Qian et al., 2020). Increased levels of LysoPC (14:0), LysoPC (16:0) and LysoPE (16:0) were observed in the liver from FLHS group, which might indicate the disturbance in glycerophospholipid metabolism and increase the risk of FLHS. In the liver of layers from FLHS group, glutathione and oxidized glutathione were increased and decreased, respectively. Glutathione peroxidase catalyzes the conversion of glutathione to oxidized glutathione to reduce oxidative damage. As reported in previous studies, the activity of glutathione peroxidase was inhibited in liver and ovary of hens with FLHS (Xing et al., 2020). Inhibition of glutathione peroxidase might be the reason for the changes of glutathione and oxidized glutathione, which revealed that homeostasis of redox state was disorganized in the development of FLHS.

Decreased level of ARA in the liver of FLHS layers was observed in this study. ARA and its derivatives are involved in episode of many diseases such as obesity, diabetes, NAFLD and atherosclerosis (Sonnweber et al., 2018). Recent evidence has confirmed patients with cardiovascular disease have lower AA concentration than normal healthy control population, which contribute to increasing cardiovascular risks (Das, 2008). Moreover, ARA was found to be down-regulated in the rats with NAFLD (Xu et al., 2019). In addition, we noticed that PGF2α, PGD2, PDE2, 12S-HETE, and 15S-HETE were increased in the FLHS group. ARA is enzymatically converted into prostaglandins through the action of cyclooxygenase pathway, and into hydroxyeicosatetraenoic acids through lipoxygenase pathway. Evidence indicates that the long-term high-fat feeding can up-regulate the expression of cyclooxygenase-2 and lipoxygenase-5 in goose or rat with fatty liver (Ibrahim et al., 2011; Zhao et al., 2019). Therefore, it is speculated that, under the conditions of fatty liver, overexpressed cyclooxygenase and lipoxygenase accelerate the conversion of ARA, which resulted in low level of ARA and high levels of ARA derivative metabolites such as PGD2, PDE2, and 12S-HETE. There is a close relationship between FLHS and inflammatory response that proinflammatory cytokines including interleukin (IL)-1α, IL-1β, IL-6 and tumor necrosis factor-α were highly expressed (Xing et al., 2020). ARA and its derivatives make significant contribution to the development of inflammation (Innes and Calder, 2018). Therefore, the disturbance of ARA metabolism might be the cause for the inflammation occurred in the FLHS.

It was important to notice that the present study had some limitations. First, some ARA metabolites such as leukotrienes were not detected by the LC-MS method used in the present study. A comprehensive quantitative analysis of ARA metabolites could provide more detailed information of AA metabolism. Second, the biological functions of the liver metabolites identified by metabolomics analysis in FLHS remains unclear. Further studies are needed to explicate the action mechanism of these metabolites in laying hens with FLHS. Thirdly, because of the small number of the experimental layers used in this study, the changes in liver metabolomic profile and ARA metabolism are needed to be validated by large scale samples.

In conclusion, with the application of UPLC-QTOF/MS based metabolomics approach, 42 liver metabolites involving in glucose metabolism, amino acid metabolism, fatty acid metabolism, glycerophospholipid metabolism, and ARA metabolism were identified as potential biomarkers associated with the pathophysiology of FLHS, and the pathway analysis found that ARA metabolism might play a vital role in FLHS. In addition, the levels of some ARA metabolites such as 12S-HETE, 15S-HETE, PGF2α, PGD2, and PGE2 were increased in FLHS layers. This might suggest that ARA metabolism in liver was disordered with the development of FLHS in laying hens. Taken together, disturbance of liver metabolites and ARA derivatives were linked to the progression of FLHS, which provided a new sight for understanding the pathogenesis of FLHS from the perspective of liver metabolites.

ACKNOWLEDGMENTS

We would like to thank the technical assistance of Shanghai Applied Protein Technology Co. Ltd. This work was supported by Hebei Layer and Broiler Innovation Team of Modern Agro-industry Technology Research System (HBCT2018150210).

DISCLOSURES

The authors declare no conflicts of interest.

SUPPLEMENTARY MATERIALS

Supplementary material associated with this article can be found in the online version at doi:10.1016/j.psj.2021.101320.

REFERENCES

Arendt, B. M., E. M. Comelli, D. W. Ma, W. Lou, A. Teterina, T. Kim, S. K. Fung, D. K. Wong, I. McGilvray, S. E. Fischer, and J. P. Allard. 2015. Altered hepatic gene expression in nonalcoholic fatty liver disease is associated with lower hepatic n-3 and n-6 polyunsaturated fatty acids. Hepatology 61:1565–1578.

Das, U. N. 2008. Essential fatty acids and their metabolites could function as endogenous HMG-CoA reductase and ACE enzyme inhibitors, anti-arrhythmic, anti-hypertensive, anti-atherosclerotic, anti-inflammatory, cytoprotective, and cardioprotective molecules. Lipids Health Dis 7:37.

de Bari, L., A. Atlante, T. Armeni, and M. P. Kalapos. 2019. Synthesis and metabolism of methylglyoxal, S-D-lactoylglutathione and D-lactate in cancer and Alzheimer's disease. Exploring the crossroad of eternal youth and premature aging. Ageing Res. Rev. 53:100915.

Gao, X., P. Liu, C. Wu, T. Wang, G. Liu, H. Cao, C. Zhang, G. Hu, and X. Guo. 2019. Effects of fatty liver hemorrhagic syndrome on the AMP-activated protein kinase signaling pathway in laying hens. Poult. Sci. 98:2201–2210.

Guo, C., J. Ma, Q. Zhong, M. Zhao, T. Hu, T. Chen, L. Qiu, and L. Wen. 2017. Curcumin improves alcoholic fatty liver by inhibiting fatty acid biosynthesis. Toxicol. Appl. Pharmacol. 328:1–9.

Guo, L., J. Kuang, Y. Zhuang, J. Jiang, Y. Shi, C. Huang, C. Zhou, P. Xu, P. Liu, C. Wu, G. Hu, and X. Guo. 2021. Serum metabolomic profiling to reveal potential biomarkers for the diagnosis of fatty liver hemorrhagic syndrome in laying hens. Front. Physiol. 12:590638.

Ha, T. S., T. G. Shin, I. J. Jo, S. Y. Hwang, C. R. Chung, G. Y. Suh, and K. Jeon. 2016. Lactate clearance and mortality in septic patients with hepatic dysfunction. Am. J. Emerg. Med. 34:1011–1015.

Hadley, K. B., A. S. Ryan, S. Forsyth, S. Gautier, and N. J. Salem. 2016. The essentiality of arachidonic acid in infant development. Nutrients 8:216.

Hamid, H., J. Y. Zhang, W. X. Li, C. Liu, M. L. Li, L. H. Zhao, C. Ji, and Q. G. Ma. 2019. Interactions between the cecal microbiota and non-alcoholic steatohepatitis using laying hens as the model. Poult. Sci. 98:2509–2521.

Hsu, J. H., J. R. Wu, S. F. Liou, H. M. Chen, Z. K. Dai, I. J. Chen, and J. L. Yeh. 2011. Labedipinedilol-A prevents lysophosphatidylcholine-induced vascular smooth muscle cell death through reducing reactive oxygen species production and anti-apoptosis. Atherosclerosis 217:379–386.

Ibrahim, M., E. Farghaly, W. Gomaa, M. Kelleni, and A. M. Abdelrahman. 2011. Nitro-aspirin is a potential therapy for nonalcoholic fatty liver disease. Eur. J. Pharmacol. 659:289–295.
Innes, J. K., and P. C. Calder. 2018. Omega-6 fatty acids and inflammation. Prostaglandins Leukot Essent Fatty Acids 132:41–48.
Jeppesen, J. B., C. Mortensen, F. Bendtsen, and S. Møller. 2013. Lactate metabolism in chronic liver disease. Scand. J. Clin. Lab. Invest. 73:293–299.
Johnson, C. H., J. Ivanisevic, and G. Siuzdak. 2016. Metabolomics: beyond biomarkers and towards mechanisms. Nat. Rev. Mol. Cell Biol. 17:451–459.
Lee, B. K., J. S. Kim, H. J. Ahn, J. H. Hwang, J. M. Kim, H. T. Lee, B. K. An, and C. W. Kang. 2010. Changes in hepatic lipid parameters and hepatic messenger ribonucleic acid expression following estradiol administration in laying hens (Gallus domesticus). Poult. Sci. 89:2660–2667.
Liu, Y. T., J. B. Peng, H. M. Jia, D. Y. Cai, H. W. Zhang, C. Y. Yu, and Z. M. Zou. 2014. UPLC-Q/TOF MS standardized Chinese formula Xin-Ke-Shu for the treatment of atherosclerosis in a rabbit model. Phytomedicine 21:1364–1372.
Liu, Y., H. Tang, X. Liu, H. Chen, N. Feng, J. Zhang, C. Wang, M. Qiu, J. Yang, and X. Zhou. 2019. Frontline science: reprogramming COX-2, 5-LOX, and CYP4A-mediated arachidonic acid metabolism in macrophages by salidroside alleviates gouty arthritis. J. Leukocyte Biol. 105:11–24.
Liu, Z., M. Liu, M. Fan, S. Pan, S. Li, M. Chen, and H. Wang. 2021. Metabolomic-proteomic combination analysis reveals the targets and molecular pathways associated with hydrogen sulfide alleviating NAFLD. Life Sci. 264:118629.
Lu, H., X. Yuan, Y. Zhang, M. Han, S. Liu, K. Han, P. Liang, and J. Cheng. 2020. HCBP6 deficiency exacerbates glucose and lipid metabolism disorders in non-alcoholic fatty liver mice. Biomed. Pharmacother. 129:110347.
Middendorf, L., D. Radko, K. Düngelhoef, E. Sieverding, H. Windhaus, D. Mischok, and C. Visscher. 2019. Amino acid pattern in the liver and blood of fattening turkeys suffering from hepatic lipidosis. Poult. Sci. 98:3950–3962.
Qian, M., H. Hu, Y. Yao, D. Zhao, S. Wang, C. Pan, X. Duan, Y. Gao, J. Liu, Y. Zhang, S. Yang, L. W. Qi, and L. Wang. 2020. Coordinated changes of gut microbiome and lipidome differentiates nonalcoholic steatohepatitis (NASH) from isolated steatosis. Liver Int. 40:622–637.
Saely, C., D. Zanolin, A. Vonbank, A. Leiherer, P. Rein, P. Schwerzler, A. Mader, and H. Drexel. 2017. Nonalcoholic fatty liver disease in coronary artery disease patients-association with impaired glucose metabolism and with future cardiovascular event risk. Atherosclerosis 263:e255.
Shini, A., S. Shini, and W. L. Bryden. 2019. Fatty liver haemorrhagic syndrome occurrence in laying hens: impact of production system. Avian Pathol. 48:25–34.
Shini, S., A. Shini, and W. L. Bryden. 2020. Unravelling fatty liver haemorrhagic syndrome: 2. Inflammation and pathophysiology. Avian Pathol. 49:131–143.
Sonnweber, T., A. Pizzini, M. Nairz, G. Weiss, and I. Tancevski. 2018. Arachidonic acid metabolites in cardiovascular and metabolic diseases. Int. J. Mol. Sci. 19.
Sztolsztener, K., A. Chabowski, E. Harasim-Symbor, P. Bielawiec, and K. Konstantynowicz-Nowicka. 2020. Arachidonic acid as an early indicator of inflammation during non-alcoholic fatty liver disease development. Biomolecules 10:1133.
Tallima, H., and R. R. El. 2018. Arachidonic acid: physiological roles and potential health benefits - a review. J. Adv. Res. 11:33–41.
Trott, K. A., F. Giannitti, G. Rimoldi, A. Hill, L. Woods, B. Barr, M. Anderson, and A. Mete. 2014. Fatty liver hemorrhagic syndrome in the backyard chicken: a retrospective histopathologic case series. Vet. Pathol. 51:787–795.
Wang, S. H., W. W. Wang, H. J. Zhang, J. Wang, Y. Chen, S. G. Wu, and G. H. Qi. 2019. Conjugated linoleic acid regulates lipid metabolism through the expression of selected hepatic genes in laying hens. Poult. Sci. 98:4632–4639.
Wang, T., K. Chen, W. Yao, R. Zheng, Q. He, J. Xia, J. Li, Y. Shao, L. Zhang, L. Huang, L. Qin, M. Xu, Z. Zhang, D. Pan, Z. Li, and F. Huang. 2021. Acetylation of lactate dehydrogenase B drives NAFLD progression by impairing lactate clearance. J. Hepatol. 74:1038–1052.
Xing, C., Y. Wang, X. Dai, F. Yang, J. Luo, P. Liu, C. Zhang, H. Cao, and G. Hu. 2020. The protective effects of resveratrol on antioxidant function and the mRNA expression of inflammatory cytokines in the ovaries of hens with fatty liver hemorrhagic syndrome. Poult. Sci. 99:1019–1027.
Xu, S., Z. Liu, and P. Liu. 2013. HDL cholesterol in cardiovascular diseases: the good, the bad, and the ugly? Int. J. Cardiol. 168:3157–3159.
Xu, Y., J. Han, J. Dong, X. Fan, Y. Cai, J. Li, T. Wang, J. Zhou, and J. Shang. 2019. Metabolomics characterizes the effects and mechanisms of quercetin in nonalcoholic fatty liver disease development. Int. J. Mol. Sci. 20:1220.
Zhao, M. M., T. J. Liu, Q. Wang, R. Zhang, L. Liu, D. Q. Gong, and T. Y. Geng. 2019. Fatty acids modulate the expression of pyruvate kinase and arachidonate-lipoxygenase through PPARγ/CYP2C45 pathway: a link to goose fatty liver. Poult. Sci. 98:4346–4358.
Zhuang, Y., C. Xing, H. Cao, C. Zhang, J. Luo, X. Guo, and G. Hu. 2019. Insulin resistance and metabonomics analysis of fatty liver haemorrhagic syndrome in laying hens induced by a high-energy low-protein diet. Sci. Rep. 9:10141.